ACS APPLIED MATERIALS & INTERFACES

Research Article

www.acsami.org

Hierarchical Nanohybrids with Porous CNT-Networks Decorated Crumpled Graphene Balls for Supercapacitors

By Shun Mao,[†,§] Zhenhai Wen,[†,§] Zheng Bo,[‡] Jingbo Chang,[†] Xingkang Huang,[†] and Junhong Chen*[,†]

[†]Department of Mechanical Engineering, University of Wisconsin-Milwaukee, 3200 North Cramer Street, Milwaukee, Wisconsin 53211, United States

[‡]State Key Laboratory of Clean Energy Utilization, Institute for Thermal Power Engineering, Department of Energy Engineering, Zhejiang University, 38 Zheda Road, Hangzhou, Zhejiang Province 310027, China

Supporting Information

ABSTRACT: One of the most challenging issues in developing supercapacitor technology is the rational design and synthesis of active electrode materials, at the nanoscale, with favorable morphologies, reasonable porous structure, and excellent conductivity. By transforming a two-dimensional (2D) graphene sheet into a crumpled ball shape, a novel three-dimensional (3D) graphene structure with a large surface area and aggregation-resistant properties has been proposed as an active material in supercapacitors to address the issues associated with the restacking of 2D graphene sheets. To further improve the mass transport/electron transfer and address the issue of limited contact spots between the crumpled graphene balls (CGBs) or between the CGBs and the current collector, we report here a unique hierarchical nanohybrid with porous carbon nanotube (CNT)-networks decorated CGBs (p-CNTn/CGBs), which not only greatly improves the affinity for bridging the active material and the current collector but also maintains favorable features for supercapacitor applications, such as a large surface area, 3D hierarchical nanostructure, excellent electrical conductivity, and outstanding aggregation-resistance. The performance established on the p-CNTn/CGBs far exceeded the bare CGB and reduced graphene oxide (RGO) counterparts in terms of specific capacitance and rate capabilities.

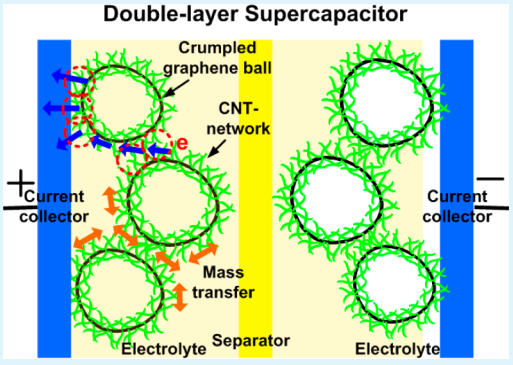

KEYWORDS: *crumpled graphene ball, carbon nanotube, hierarchical nanohybrid, supercapacitor*

INTRODUCTION

Graphene, a two-dimensional (2D) carbon structure, is of great interest for fundamental scientific research and practical technological applications due to its prominent structural and electrical properties.[1−3] Because of its high electric conductivity, large specific surface area, and excellent chemical/mechanical stability,[4−6] graphene has been widely studied as an electrode material in supercapacitors, a type of energy storage device with high capacitance and powder density, bridging the gap between conventional capacitors and rechargeable batteries.[7−14] Graphene can be produced by various approaches,[15−17] and producing graphene through reduced graphene oxide (RGO) is a promising route for developing commercial supercapacitors, as it can be synthesized in large quantities by oxidizing inexpensive graphite powders followed by reduction through a variety of methods.[18−21] However, due to the 2D nature of the graphene sheet, graphene can easily restack to form lamellar microstructures on the current collector during the electrode fabrication process. The restacking of the graphene sheets may greatly reduce the utilization of the electrode material and limit the electron and mass transport at the interface of electrode, which as a result leads to decreased capacitor performance.[22]

Crumpled graphene balls (CGB), a new type of carbon with a crumpled sphere structure of the graphene sheet, have recently been produced from aqueous graphene oxide (GO) nanosheets by capillary force associated with rapid drying of the solvent and physical deformation through an aerosolization process.[23−30] This process could transfer the graphene from a 2D sheet to a 3D crumpled structure, which has higher specific surface area than the stacked 2D graphene sheets.[23] Of more interest, the CGB structure is rigid and can easily sustain its structure after being immersed in an electrolyte solution and is remarkably aggregation-resistant.[23] Though the CGB structure contains a lot of advantages, there is still a need to further improve its efficiency in mass transport, electron transfer, and utilization. On one hand, it is reasonable to predict that the contact spots between the CGBs or between the CGBs and the current collector, due to their crumpled ball shape, are limited when used as the electrode material in a supercapacitor, because a constriction/spreading resistance inevitably forms between the two surfaces meeting at a limited number of contact spots for charge transport.[31] On the other hand, the mass transport, that is, ions or electrolyte, at the interface of the electrode can be impeded because of the tight stacking of CGBs. This is why

Received: April 29, 2014
Accepted: May 6, 2014
Published: May 6, 2014

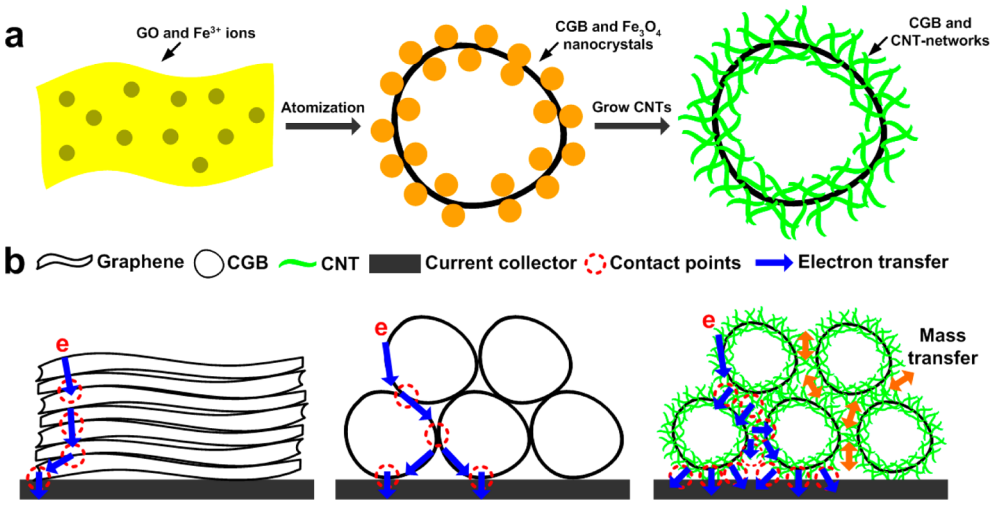

Figure 1. (a) Schematic illustration of the p-CNTn/CGB hybrid preparation method. (b) Schematic illustrations of electron transport between the flat graphene, CGBs, and p-CNTn/CGB hybrids and current collector, respectively.

CGB-based supercapacitors usually show low rate capabilities with significant drops in capacitance under high discharge currents.[32]

Taking these points into consideration, we herein report a carbon nanotube (CNT)/CGB hybrid by direct growth of CNTs on the CGB surface. Unlike previously reported CNT/graphene hybrids,[33−39] the present hybrid has a unique hierarchical structure because the CGB surface is decorated with porous CNT-networks (p-CNTn) and thus has a variety of advantages for supercapacitor applications, as show in Figure 1. Above all, in such a unique hierarchical hybrid structure, the out-stretched tips of the CNTs offer multiple conducting channels to improve the charge transfer between the CGBs and between the CGBs and the current collector. In addition, the porous networks constructed by the CNTs afford easy and quick channels for mass (e.g., ion and electrolyte) transport. Moreover, the CGB structure, benefiting from its rigidity, guarantees the stability of the 3D hierachical structure. Based on systematic electrochemical testing, the p-CNTn/CGBs, in comparison with pure CGB and RGO sheets, showed enhanced specific capacitance (202.0 F/g at a current density of 0.325 A/g), significantly improved rate capabilities (48−65% retention with more than two-order increase in the discharge current density or scan rate), and considerable energy density (2.72 Wh/kg) even at a high current density of 65 A/g.

RESULTS AND DISCUSSION

The p-CNTn/CGB hybrids were synthesized through a two-step process, as shown in Figure 1a. In the first step, CGB/Fe_3O_4 nanocrystal hybrids were produced by our previously reported one-pot ultrasonic nebulizer-based spray method.[26,27] Specifically, the GO suspension with precursor ions (i.e., Fe^{3+}) was nebulized to generate aerosol droplets that flowed through a tube furnace. Because the average size of the generated droplets was on the order of micrometers, the solvents rapidly evaporated in the tube furnace, leading to the shrinkage of the GO sheets and the subsequent compression of the GO sheets into crumpled balls with a submicrometer size. Simultaneously, Fe_3O_4 nanocrystals grew from the precursor Fe^{3+} ions and deposited on both external and internal surfaces of the CGBs during the solvent evaporation and the GO crumpling process. In the second step, CNTs were grown on the CGB surface through a chemical vapor deposition (CVD) method with Fe as the catalyst. The typical growth process included a reduction of the CGB/Fe_3O_4 hybrids with H_2 and a CVD growth of CNTs with C_2H_2 gas as the carbon source.

The pure CGBs, the CGB/Fe_3O_4, and the p-CNTn/CGB hybrids were characterized by scanning electron microscopy (SEM) and transmission electron microscopy (TEM) (Figure 2). The pure CGBs were synthesized from a monolayer GO suspension without precursor ions and generally have a near-spherical shape with a 3D morphology from wrinkled and folded graphene sheets, as shown in Figure 2a and d. From a previous report,[23] Brunauer−Emmett−Teller (BET) specific surface area of heated CGBs is around 587 m^2/g, which is much larger than the lamellar GO sheets and can retain its large specific surface area after compression (255 m^2/g) and solution processing (410 m^2/g). Therefore, the 3D CGB structure is attractive for supercapacitor electrodes due to its large specific surface area and aggregation-resistant nature. By adding Fe^{3+} ions to the GO suspension, CGB/Fe_3O_4 hybrids were produced, and SEM images show that Fe_3O_4 nanocrystals were uniformly deposited on the surface of the CGB structure (Figure 2b and e), indicating the local growth of nanocrystals during the GO aerosolization and crumpling process. X-ray diffraction (XRD) was conducted to study the crystallographic structure of the CGB/Fe_3O_4 hybrid (Supporting Information, Figure S2b), which shows a good crystalline structure of Fe_3O_4 nanocrystals and a decreased interlayer spacing of the CGBs (3.7 Å, 23°) compared with GO (8.32 Å, 10.6°),[40] indicating the CGB structure is formed by crumpled RGO sheets.

The Fe_3O_4 nanocrystals were then reduced to iron nanocrystals and used as the catalyst for CVD growth of CNTs. The successful creation of the p-CNTn/CGB hybrid structure was evidenced by SEM and TEM images, as shown in Figure 2. With a 3 min reduction of the CGB/Fe_3O_4 hybrids and a 1 min growth of CNTs, the product CNTs had a diameter of 15-25 nm and a length in the range of a few dozen to several hundred nanometers. The high-resolution TEM (HRTEM) images show that the CNTs are multi-walled CNTs with 10−15 layers. Based on the SEM and TEM images, the CNTs on the CGB surface were found to be interconnected to form a porous network with lots of CNT tips stretched out to CGBs, which is an ideal structure to bridge the CGBs and the current collector.

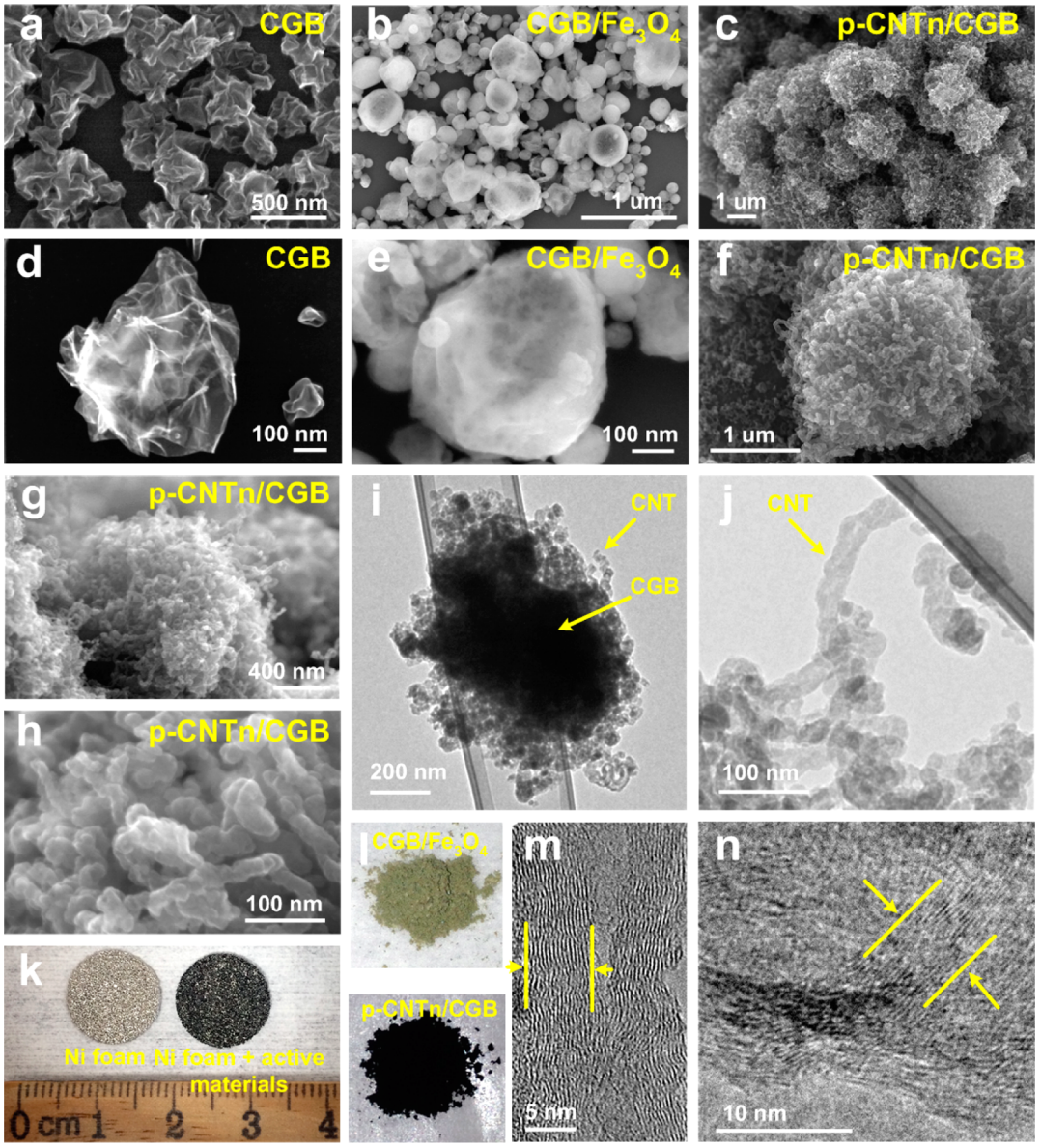

Figure 2. SEM images of (a, d) CGBs, (b, e) CGB/Fe_3O_4 hybrids, and (c, f, g, h) p-CNTn/CGB hybrids. (i, j, m, n) TEM and high-resolution TEM images of p-CNTn/CGB hybrids. The CNTs on the CGB surface have a diameter of 15−25 nm and a length in the range of few dozen to several hundred nanometers. (k) Digital images of the bare Ni foam and Ni foam coated with active materials. (l) Digital images of the CGB/Fe_3O_4 and p-CNTn/CGB powders.

After the active materials are compressed to the current collector, it is believed that the CNT-networks will greatly increase the contact spots between the CGBs and the current collector. Notably, iron nanocrystals were found in the hybrids based on the TEM images and could be removed by acid treatment after the CNT growth. The good crystallinity of the CGB and CNT in the p-CNTn/CGB hybrids were verified by Raman spectroscopy (Supporting Information, Figure S2c), and the results show that defects were presented in the hybrids because the CGB was formed from the reduction and crumpling of GO and some defects (sp^3 carbon) were introduced into the CNTs during the growth. The BET specific surface area of the p-CNTn/CGB hybrids was tested (Supporting Information, Figure S2d). The p-CNTn/CGB hybrids have a BET surface area of 260.0 m^2/g with a pore volume and average pore size of 0.28 cm^3/g and 4.7 nm, respectively. It should be noted that the BET surface area of the p-CNTn/CGB hybrids is smaller than that of the CGBs (587 m^2/g), because the hybrids are constructed by CGB and CNTs with few residual iron nanocrystals.

CNTs on the CGB surface are favorable for supercapacitors because the CNTs could work as both active materials and conducting channels to improve the contact for charge transfer between the CGBs and the current collector. As demonstrated in Figure 1b, for flat graphene sheets and CGBs, there are a limited number of contact spots at the contact interfaces among the active materials and between the active materials and the current collector. For these cases, electrons have to travel a long way to reach, go through, and spread into the current collector during the charge/discharge processes.[41] The considerable constriction/spreading resistance will certainly affect the capacitor performance as a result of an obstructive electron transport, especially when running at high discharge rates. In contrast, as shown in Figure 1b, with CNT-networks bridging the active materials and the current collector, the tips and sidewalls of the

dx.doi.org/10.1021/am502604u | ACS Appl. Mater. Interfaces 2014, 6, 9881−9889

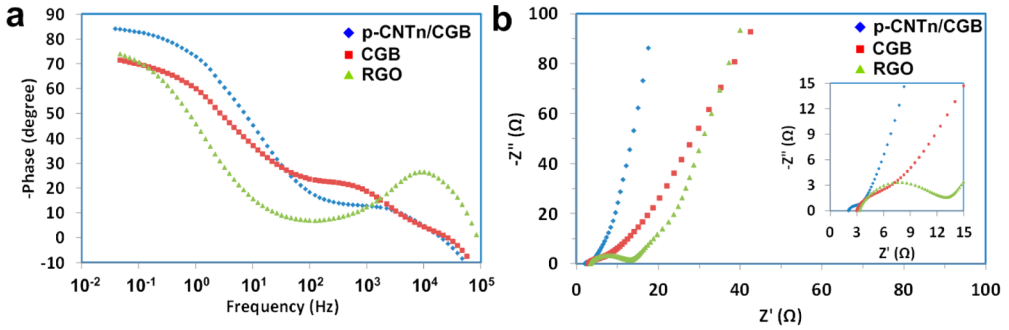

Figure 3. (a) Phase responses as a function of frequency of the p-CNTn/CGB, CGB, and RGO cells. (b) Nyquist plots of the p-CNTn/CGB, CGB, and RGO cells, showing the imaginary part versus the real part of impedance. Inset shows the data at high-frequency ranges.

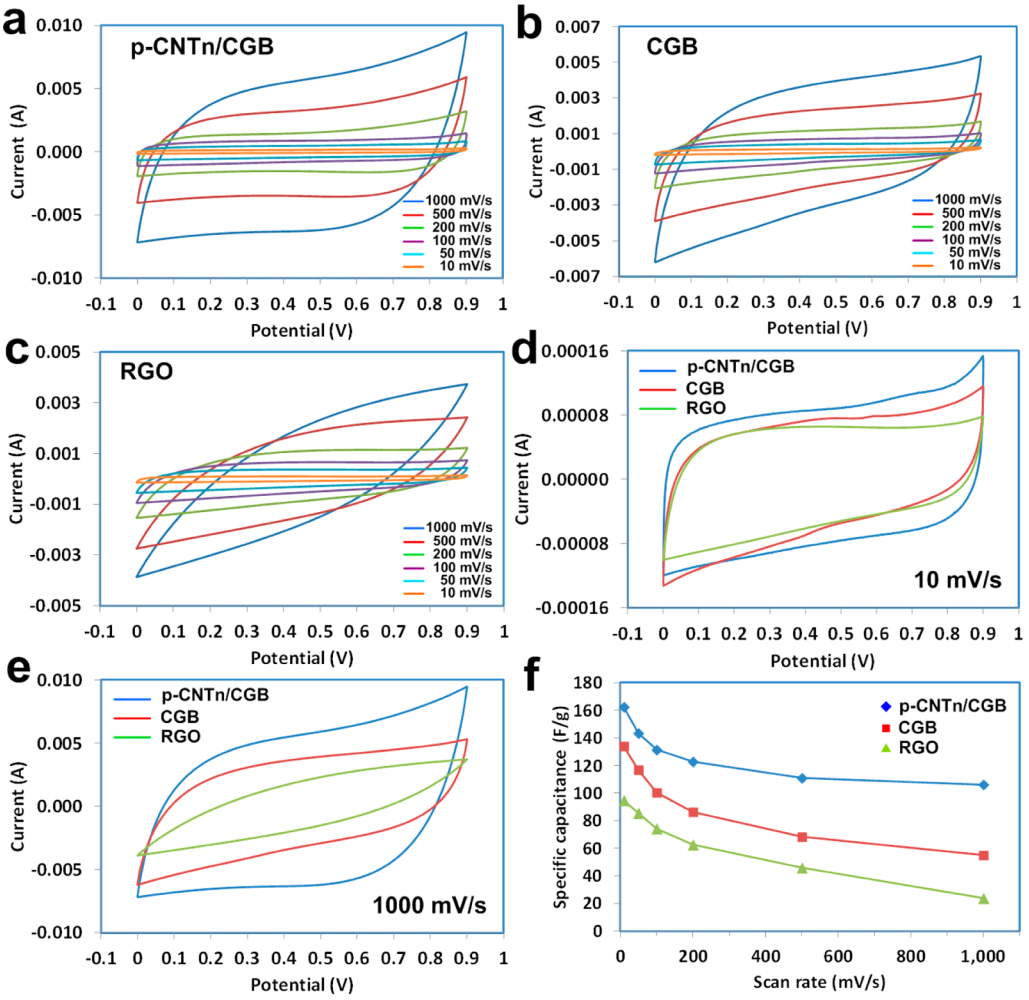

Figure 4. Double-layer electric capacitor performance of the p-CNTn/CGB, CGB, and RGO cells with a loading of 0.13, 0.12, and 0.22 mg/cm^2, respectively. Electrolyte: 6 M KOH aqueous solution. (a, b, and c) CVs of the p-CNTn/CGB, CGB, and RGO cells at different scan rates from 10 to 1000 mV/s, respectively. (d) CVs of different cells at a scan rate of 10 mV/s. (e) CVs of different cells at a scan rate of 1000 mV/s. (f) The dependences of specific capacitances on potential scan rates of the p-CNTn/CGB, CGB, and RGO cells.

CNTs could provide numerous contact spots/pathways, significantly facilitating the electron transport during charge/discharge processes. To evaluate the performance of the p-CNTn/CGB hybrids as electrode materials in a supercapacitor, two-electrode symmetric coin cells were assembled with p-CNTn/CGB hybrids, RGO sheets, and CGBs as active materials, Ni foam as the current collector, and a 6 M KOH aqueous solution as the electrolyte.

To understand the dielectric and transport properties of the electrodes, electrochemical impedance spectroscopy (EIS) was conducted for p-CNTn/CGB-, RGO-, and CGB-based cells. Figure 3a shows the phase responses of the frequency for different cells. Both RGO and CGB cells show a phase angle of around −70° in low frequency, which is far below 90 deg, suggesting a combination of capacitor and resistor characteristics. In striking contrast to the RGO and CGB cells, the p-CNTn/CGB cell presented a phase angle of nearly −85 degree with a

dx.doi.org/10.1021/am502604u | ACS Appl. Mater. Interfaces 2014, 6, 9881−9889

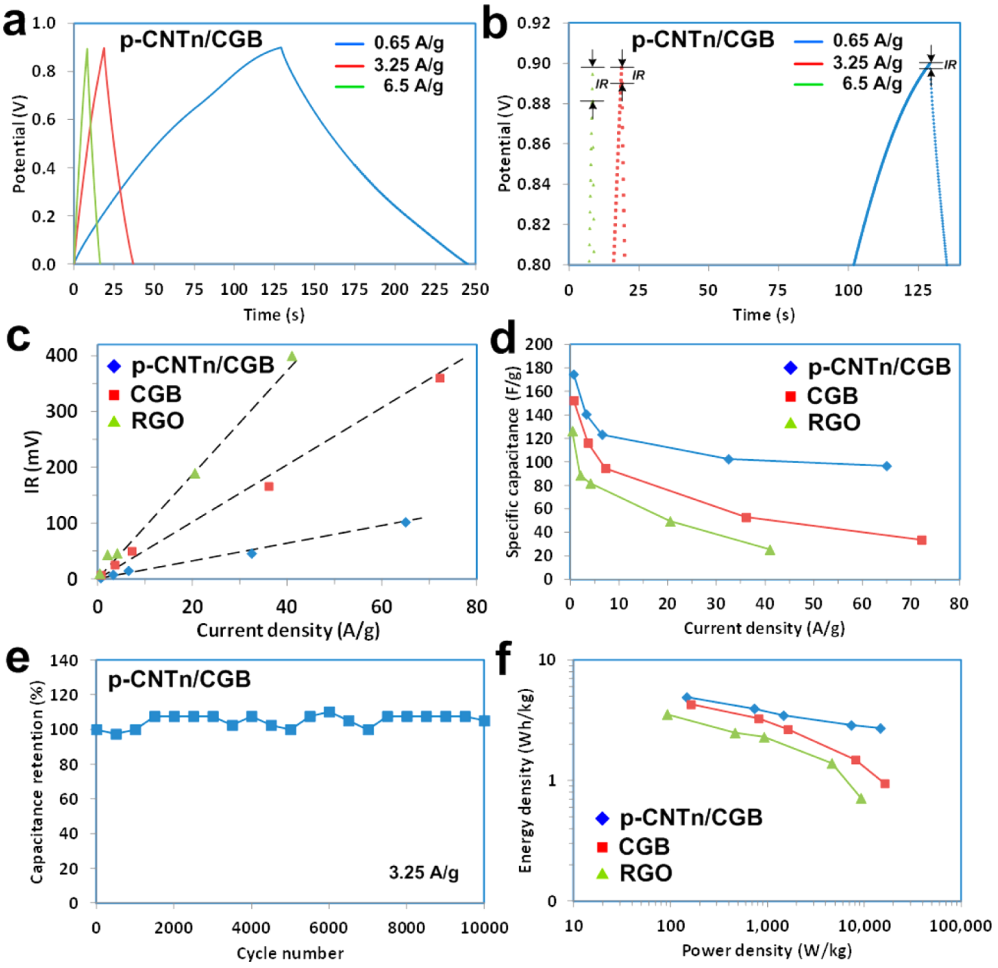

Figure 5. (a) Galvanostatic charge/discharge curves of the p-CNTn/CGB cell under different discharge current densities. The current density was calculated based on the mass of a single electrode. (b) Magnified portion at the initiation of the discharge in galvanostatic charge/discharge plots for the p-CNTn/CGB cell at different discharge current densities. (c) The *IR* drop plots of the p-CNTn/CGB, CGB, and RGO cells at different discharge current densities. (d) The dependences of the specific capacitances on discharge currents of the p-CNTn/CGB, CGB, and RGO cells. (e) Cycling performance of the p-CNTn/CGB cell tested at a current density of 3.25 A/g. (f) Ragone chart of the p-CNTn/CGB, CGB, and RGO cells.

significantly enlarged frequency range associate with a few times/one order of magnitude higher knee frequency (the maximum frequency at which the capacitive storage of electrical energy is dominant), suggesting an excellent capacitive feature.[42] Figure 3b shows the Nyquist plots for various symmetric cells in the frequency range from 0.05 Hz to 500 000 Hz measured at equilibrium open circuit potential (0 V) with 10 mV amplitude. The Nyquist plot is almost a vertical line for the p-CNTn/CGB cell, indicating a more facile electrolyte diffusion and ion transport and nearly ideal capacitive behavior of the electric double-layer capacitor. In addition, the p-CNTn/CGB cell, different from the other two counterpart cells, almost shows a negligible semicircle in the higher frequency region. The negligible semicircle, which represents the frequency-dependent ion diffusion resistance towards the electrode surface, further demonstrates a relatively faster diffusion of ions or smaller diffusion resistance at the interface of the p-CNTn/CGB electrode.[43] The equivalent series resistance (ESR) of the cells can be estimated according to the *x*-intercept of the Nyquist plots (inset of Figure 3b). The p-CNTn/CGB-based cell possesses the smallest ESR value among the three cells, confirming our assumption that the decoration of p-CNTn on CGBs could improve electrical conductivity.

The electrochemical capacitive properties of the cell were first characterized by a cyclic voltammetry (CV) test. Parts a, b, and c of Figure 4 show the CVs of p-CNTn/CGB-, CGB-, and RGO-based supercapacitors at different scan rates from 10 to 1000 mV/s, respectively. For the p-CNTn/CGB cell, the CV basically maintained its rectangular shape as the scan rate increased, which is completely different from the CGB and RGO cells that show distinct distorted shapes at a high scan rate. To make a close comparison among the three cells, CVs at low scan rate (10 mV/s) and high scan rate (1000 mV/s) are shown in Figure 4d and e, respectively. At a low scan rate, CVs from all cells have a nearly rectangular shape, indicating good capacitor characteristics (Figure 4d). However, by carefully viewing the transition parts connecting the reverse sweeps at around 0 and 0.9 V potentials, it was found that the slopes of $\Delta I/\Delta V$ of the p-CNTn/CGB cell is larger than those of the RGO and the CGBs, which indicates better charge/discharge-rate responses of the p-CNTn/CGB cell to the applied potential.[44] This trend becomes more significant when the scan rate increases, as shown in Figure 4e; the shapes of the CVs for RGO and CGBs are greatly distorted when the scan rate reaches 1000 mV/s. As a comparison, with an increase in scan rate, the p-CNTn/CGB cell still maintained a well rectangular shape of the CV curve. All of these results demonstrated that the p-CNTn/CGB cell possessed a better

dx.doi.org/10.1021/am502604u | *ACS Appl. Mater. Interfaces* 2014, 6, 9881−9889

rate performance. The specific capacitance of single electrode of the cells was calculated based on the scan rates and response currents in the CV curves (Supporting Information, capacitor performance calculations). As shown in Figure 4f, the p-CNTn/CGB cell shows a specific capacitance of 162.3 F/g at 10 mV/s, which decreased to 106.1 F/g (34.7% decrease) when the scan rate increased to 1000 mV/s. In contrast, the specific capacitances of the CGBs and the RGO sheets showed much larger decreases of 59.0% (from 133.9 F/g to 54.9 F/g) and 74.9% (from 94.6 F/g to 23.8 F/g) when the scan rate increased from 10 mV/s to 1000 mV/s, respectively. The results from the CV tests have further proved that by using a porous CNT network as the conducting channel between the CGBs and the current collector, both the specific capacitance and the rate capabilities of the supercapacitor are greatly improved.

A galvanostatic current charge/discharge test was also used to evaluate the supercapacitor performance of the cells. Figure 5a shows the typical charge/discharge curves of the supercapacitor based on p-CNTn/CGBs with the current density range 0.325−65 A/g. The charge/discharge curves displayed an isosceles triangle shape without plateaus, indicating the electrochemical double-layer capacitance behavior of the p-CNTn/CGB. The charge/discharge curves of the RGO and CGB cells also showed similar isosceles triangle shapes, but with a decreased discharge time at similar current densities (Supporting Information, Figure S3), demonstrating a higher capacity achieved in p-CNTn/CGB cell. Figure 5b shows the magnified galvanostatic charge/discharge plots in the high-potential range (0.8−0.9 V) for the p-CNTn/CGB cell at different current densities. Small voltage (*IR*) drops for all discharge curves are found, which arise from the intrinsic internal resistance of the supercapacitor. The *IR* drops were plotted with different current densities to compare the *IR* drops among the p-CNTn/CGB, CGB, and RGO cells, as shown in Figure 5c. It was found that the *IR* drops of the p-CNTn/CGB cell were much smaller than those of the CGB and RGO cells and this trend was more significant at higher current densities. The slopes of the linear fitting lines, representing the constant internal resistance of the supercapacitor, indicate that the p-CNTn/CGB cell had much smaller internal resistance than the CGB and RGO cells. Such significantly reduced *IR* drop/internal resistance can be attributed to the CNT-bridged high-quality contact at the interface of the active materials and the current collector.

The specific capacitance of single electrode of the cells was calculated from galvanostatic discharge curves as shown in Figure 5d. The specific capacitances were similar to those calculated from the CV tests and decreased with the increasing discharge current densities. As expected, the specific capacitance of the p-CNTn/CGB cell showed much less decrease at a high discharge current density. As shown in Figure 5d, the specific capacitance of the p-CNTn/CGB cell decreased 52.1% from 202.0 F/g to 96.7 F/g when the current density increased from 0.325 to 65 A/g, while the specific capacitances of the CGB and RGO cells decreased 80.9% from 176.4 F/g to 33.7 F/g and 81.2% from 135.6 F/g to 25.5 F/g, respectively, when the current density increased for two hundred times. The results from the galvanostatic current charge/discharge tests are in accordance with the CV results and further confirm that the p-CNTn/CGB hybrids had higher rate capabilities than the RGO and CGBs. The cycling properties of the p-CNTn/CGB capacitor were studied by charging and discharging the device with a constant current density of 3.25 A/g. The capacitance retention results (Figure 5e) show that the specific capacitance of the p-CNTn/CGB capacitor retained the initial capacitance value even after 10 000 cycles with small fluctuations in the range from 97.4 to 107.7%. The fluctuations are believed coming from the relative large charge/discharge current density, and become much smaller after 7500 cycles (∼2.6%). The cycling test results suggest that the p-CNTn/CGBs are mechanically and chemically stable as active materials in supercapacitors.

The Ragone plots shown in Figure 5f further demonstrate the excellent rate performance of the p-CNTn/CGB cell with high energy and power densities. The p-CNTn/CGB cell showed a reasonable energy density of 4.9 Wh/kg at a power density of 0.15 kW/kg and remained at 2.7 Wh/kg at a high power density of 14.6 kW/kg. This energy density is comparable to commercially available carbon/carbon devices from several companies, 1.1 to 9.2 Wh/kg with a powder density of 0.15 to 2 kW/kg, and also prototype devices using activated carbon, 4.2 to 5.3 Wh/kg with a power density of 0.9 to 8.3 kW/kg.[45] The maximum energy density value of the p-CNTn/CGB cell (4.9 Wh/kg) is higher than that of the CGB (4.3 Wh/kg) and RGO (3.4 Wh/kg); the p-CNTn/CGB cell shows a better energy density retention at higher discharge current densities, indicating improved rate performance. The relatively low energy density, compared to previously reported graphene-based aqueous supercapacitors, for example, activated porous graphene-based supercapacitor,[14] is due to the relatively low specific surface area (260 m^2/g compared to 3100 m^2/g) of our materials. However, the CGB was produced from untreated GO. Therefore, by using GO of higher specific surface area, for example, microwave-exfoliated GO, and proper activation method, for example, activation with KOH, the specific surface area of CGB could be enhanced and an increase in the energy density of our materials is expected.

For the reliable and accurate evaluation of the capacitor performance and to study the impact from the loading of the active materials to the capacitor performance, p-CNTn/CGB cells with different loadings (0.15 to 1.3 mg or 0.13 to 1.15 mg/cm^2) of active materials on each electrode were prepared and tested by galvanostatic charge/discharge measurements. The specific capacitances of the cells with different loadings and discharge current densities were plotted in the Supporting Information, Figure S4a. From the plots of the specific capacitance versus the mass of active materials under different discharge currents, it was found that the cell specific capacitance decreased with the increase of the mass of active materials and the decrease in the capacitance was more significant under higher discharge currents. For instance, the capacitance of the cell decreased from 202.0 to 198.1 F/g (discharge current: 0.325 A/g) and from 140.7 to 125.6 A/g (discharge current: 3.25 A/g) when the loading increased from 0.13 to 1.15 mg/cm^2. This is consistent with previous reports[32,46,47] and is because the increased material layer thickness will increase the ion and electron transport distance/resistance and thus decrease the specific capacitance of the cell. Compared with previous reports, the capacitance retention of the p-CNTn/CGB cells is very high (89.3 to 98.1%) when the loading mass increases for almost night times. The high retentions of specific capacitance respect to increased loadings indicate that the 3D porous structure of the hybrids facilitates the mass and electron transport, which is an unique property and advantage of CGB-based capacitors.[32] The results of the cells with higher loadings further prove that our hybrids could potentially solve the problem of the graphene sheet restacking leaded performance loss with increased loading of the active materials.

The specific area/volume capacitance is also important for the practical application of powdery electrode materials in supercapacitors. Figures S4b and c (Supporting Information) show the calculated specific area capacitance of single electrode of the p-CNTn/CGB cells with different loadings and the comparison of specific area capacitances of the p-CNTn/CGB, CGB, and RGO cells. Based on the results, the specific area capacitance of the p-CNTn/CGB cells are in the range 0.02−0.23 F/cm^2 with various loadings and discharge currents, which are comparable to previously reported CNT and graphene-based supercapacitors.[48−50] Because the specific area capacitance was calculated with unit surface area, with a higher active material loading on unit area of the electrode, the capacitance of the cell was higher, which was found in this study and previous report.[50] By comparing the specific area capacitances of the p-CNTn/CGB, CGB, and RGO cells under different discharge current densities, similar to the specific mass capacitance, the p-CNTn/CGB hybrids showed higher rate capabilities than the RGO and the CGBs. The specific volume capacitance of the p-CNTn/CGB cells was also calculated based on the galvanostatic current charge/discharge tests and the volume of the Ni foam (Supporting Information, Figure S4d). The specific volume capacitance of the p-CNTn/CGB cells were in the range 0.81−9.59 F/cm^3 with various loadings and discharge currents and increased with the increase of loading and decrease of charge/discharge current.

Free-standing carbon structures, for example, graphene/CNT foams, graphene/CNT papers, etc., have shown their advantages in the supercapacitors as these nanostructures have high conductivity and could work as the current collector themselves. However, due to the 2D nature of the graphene sheet, graphene can easily restack to form lamellar microstructures, which is the typical structure in the free-standing carbon foams or films. As demonstrated, the formation of porous CNT-networks on the aggregation-resistant CGB structure is favorable for supercapacitor applications, because such unique architecture is of great benefit for smooth charge transfer that leads to low contact resistance and high utilization efficiency, as well as facilitating mass transport of ions and electrolyte, which finally give rise to significantly improved rate capability. So compared with free-standing carbon structures, our material represented a method to improve the rate capability of the nanocarbon-based supercapacitors and resolved restacking issues in the graphene/CNT-based free-standing carbon structures. To further study the function of the p-CNTn in the p-CNTn/CGB cell, we have also fabricated p-CNTn/CGB with larger CNTs (LCNT/CGB) of 100 nm in diameter and 2−10 μm in length. The capacitor performance of the LCNT/CGB cell was also investigated by CV and galvanostatic charge/discharge tests (Supporting Information, Figure S5). The CV of the LCNT/CGB cell had a similar shape to that of the p-CNTn/CGB cell. Based on the galvanostatic charge/discharge test, the LCNT/CGB cell also had much better rate capability (47% capacitance retention with two orders of magnitude increase in the discharge current density) than supercapacitor cells fabricated with RGO and CGBs. The results from LCNT/CGB cells further confirm the function of CNT-networks in enhancing the specific capacitance and the rate capability of CGB-based supercapacitors and the critical role of contact in designing high-performance supercapacitors.

CONCLUSIONS

To summarize, we reported a 3D carbon-based architecture, that is, porous CNT-networks decorated CGBs, as promising electrode material in supercapacitors. The 3D CGB, with a high specific surface area, microsphere morphology, and aggregation-resistant nature, leads to a high specific capacitance and stability in supercapacitors. The CNT porous networks facilitated mass transport and decreased the contact resistance between the CGBs and that between CGBs and the current collector, significantly improving the rate capability of supercapacitors. The p-CNTn/CGB cell showed a better performance than the graphene/CGB hybrids with physically mixed CGBs and graphene,[32] and its performance was also among the best reported graphene-based supercapacitors[14,37,41,51−58] (Supporting Information, Table S1). Notably, the p-CNTn/CGB supercapacitor performance could be further optimized by removing the residual iron, fine-tuning the size and loading of the CNTs, and increasing the reduction level of the CGBs. The as-designed p-CNTn/CGB structure represents a new type of carbon nanoarchitecture with a unique morphology and should be attractive for many energy device applications, for example, Li-ion batteries and fuel cells, relying on its unique structure and excellent properties.

METHODS

Synthesis of p-CNTn/CGB Hybrids. The p-CNTn/CGB hybrids were synthesized through two steps. In the first step, CGB/Fe_3O_4 hybrids were produced by a previously reported aerosolization/high-temperature-induced GO crumpling and nanocrystal growth method. In a typical procedure, $FeCl_3$ (2 mM) was added into the GO suspension (0.2 mg/mL) as the precursor for the growth of Fe_3O_4 nanocrystals. The mixed solution was nebulized by an ultrasonic nebulizer (2.4 MHz, 241T, Sonaer) to form aerosol particles, which were carried by argon gas through a horizontal tube furnace preheated at a desired temperature (750 °C). The GO sheets were quickly dried and crumpled into a 3D ball shape during flight in the tube furnace; the precursor Fe^{3+} ions led to the formation of Fe_3O_4 nanocrystals on the surface of CGB sheets. A schematic illustration of the experimental setup is shown in the Supporting Information, Figure S1. CNTs were grown on the CGB surface through a CVD method with Fe as the catalyst. The typical growth process included a thermal annealing of the CGB/Fe_3O_4 hybrids in a mixed Ar and H_2 (flow rate 3:2) atmosphere at 700 °C for 3 min and then in an H_2 and C_2H_2 (flow rate 5:1) atmosphere for 1 min. The RGO sample was prepared by thermal reduction of the GO sheets in Ar atmosphere at 300 °C for 1 h.

Structure Characterization. A Hitachi (H9000 NAR) transmission electron microscope (TEM) and a Hitachi (S-4800) scanning electron microscope (SEM) were used to characterize the structure of the prepared CGB, CGB/Fe_3O_4, and p-CNTn/CGB samples. X-ray diffraction was performed on a Scintag XDS 2000 X-ray powder diffractometer with monochromatized Cu Kα radiation (λ = 1.5418 Å). Raman spectroscopy was conducted with a Renishaw Raman microscope. N_2 adsorption-desorption measurements were carried out at 77 K using a Quantachrome Autosorb gas-sorption system.

Supercapacitor Measurements. For the supercapacitor tests, p-CNTn/CGB, CGB, and RGO-based supercapacitors were fabricated in a two-electrode system with a layered structure, and all the components were sandwiched into a coil cell device. The active materials were deposited on two pieces of Ni foam with a diameter of 1.2 cm and thickness of ~0.24 mm (after compression) with polyvinylidene fluoride (PVDF, 5%) as the binder, which were separated by a porous PVDF membrane in a 6 M KOH aqueous electrolyte solution. The electrochemical performance of the supercapacitors was tested by cyclic voltammetry, galvanostatic charge/discharge, and electrochemical impedance spectroscopy on a CHI 600 electrochemical workstation (CHI Inc., U.S.A.) and a Land Battery Tester at room temperature.

■ ASSOCIATED CONTENT

Supporting Information

Schematic illustration of the experimental setup of CGB/nanocrystal hybrids preparation; SEM image of the GO sheets; XRD spectrum of the CGB/Fe_3O_4 hybrids; Raman spectrum of the p-CNTn/CGB hybrids; BET surface area study of the p-CNTn/CGB hybrids; galvanostatic charge/discharge tests of the CGB and RGO cells; supercapacitor study of the electrodes with different loadings; specific area and volume capacitances of the cells; supercapacitor study of the LCNT/CGB; supercapacitor performance calculations; performance comparison of graphene-based supercapacitors. This material is available free of charge via the Internet at http://pubs.acs.org.

■ AUTHOR INFORMATION

Corresponding Author

*Email: jhchen@uwm.edu.

Author Contributions

§S.M. and Z.W. contributed equally.

Notes

The authors declare no competing financial interest.

■ ACKNOWLEDGMENTS

Financial support for this work was provided by the U.S. Department of Energy (DE-EE0003208) and the Research Growth Initiative Program of the University of Wisconsin-Milwaukee (UWM). The authors thank Prof. M. Gajdardziska-Josifovska for TEM access at the UWM HRTEM Laboratory, Dr. H. A. Owen for technical support with SEM analyses, and Dr. S. E. Hardcastle for technical support with the XRD test. The SEM imaging was conducted at the UWM Electron Microscope Laboratory. The XRD, Raman, and BET tests were conducted at the UWM Advanced Analysis Facility.

■ REFERENCES

(1) Geim, A. K. Graphene: Status and Prospects. *Science* **2009**, *324*, 1530−1534.

(2) Geim, A. K.; Novoselov, K. S. The Rise of Graphene. *Nat. Mater.* **2007**, *6*, 183−191.

(3) Chen, J. H.; Jang, C.; Xiao, S. D.; Ishigami, M.; Fuhrer, M. S. Intrinsic and Extrinsic Performance Limits of Graphene Devices on SiO_2. *Nat. Nanotechnol.* **2008**, *3*, 206−209.

(4) Radovic, L. R.; Bockrath, B. On the Chemical Nature of Graphene Edges: Origin of Stability and Potential for Magnetism in Carbon Materials. *J. Am. Chem. Soc.* **2005**, *127*, 5917−5927.

(5) Rao, C. N. R.; Sood, A. K.; Subrahmanyam, K. S.; Govindaraj, A. Graphene: The New Two-Dimensional Nanomaterial. *Angew. Chem. Int. Ed.* **2009**, *48*, 7752−7777.

(6) Bolotin, K. I.; Sikes, K. J.; Jiang, Z.; Klima, M.; Fudenberg, G.; Hone, J.; Kim, P.; Stormer, H. L. Ultrahigh Electron Mobility in Suspended Graphene. *Solid State Commun.* **2008**, *146*, 351−355.

(7) Bose, S.; Kuila, T.; Mishra, A. K.; Rajasekar, R.; Kim, N. H.; Lee, J. H. Carbon-Based Nanostructured Materials and Their Composites as Supercapacitor Electrodes. *J. Mater. Chem.* **2012**, *22*, 767−784.

(8) Chen, J.; Li, C.; Shi, G. Graphene Materials for Electrochemical Capacitors. *J. Phys. Chem. Lett.* **2013**, *4*, 1244−1253.

(9) Cui, S.; Mao, S.; Lu, G.; Chen, J. Graphene Coupled with Nanocrystals: Opportunities and Challenges for Energy and Sensing Applications. *J. Phys. Chem. Lett.* **2013**, *4*, 2441−2454.

(10) Dyatkin, B.; Presser, V.; Heon, M.; Lukatskaya, M. R.; Beidaghi, M.; Gogotsi, Y. Development of a Green Supercapacitor Composed Entirely of Environmentally Friendly Materials. *ChemSusChem* **2013**, *6*, 2269−2280.

(11) Hsieh, C.-T.; Hsu, S.-M.; Lin, J.-Y.; Teng, H. Electrochemical Capacitors Based on Graphene Oxide Sheets Using Different Aqueous Electrolytes. *J. Phys. Chem. C* **2011**, *115*, 12367−12374.

(12) Huang, L.; Li, C.; Shi, G. High-Performance and Flexible Electrochemical Capacitors Based on Graphene/Polymer Composite Films. *J. Mater. Chem. A* **2014**, *2*, 968−974.

(13) Zhang, L.; Shi, G. Preparation of Highly Conductive Graphene Hydrogels for Fabricating Supercapacitors with High Rate Capability. *J. Phys. Chem. C* **2011**, *115*, 17206−17212.

(14) Zhu, Y.; Murali, S.; Stoller, M. D.; Ganesh, K. J.; Cai, W.; Ferreira, P. J.; Pirkle, A.; Wallace, R. M.; Cychosz, K. A.; Thommes, M.; Su, D.; Stach, E. A.; Ruoff, R. S. Carbon-Based Supercapacitors Produced by Activation of Graphene. *Science* **2011**, *332*, 1537−1541.

(15) Huang, H.; Chen, W.; Chen, S.; Wee, A. T. S. Bottom-up Growth of Epitaxial Graphene on 6H-SiC(0001). *ACS Nano* **2008**, *2*, 2513−2518.

(16) Kim, K. S.; Zhao, Y.; Jang, H.; Lee, S. Y.; Kim, J. M.; Kim, K. S.; Ahn, J.-H.; Kim, P.; Choi, J.-Y.; Hong, B. H. Large-scale Pattern Growth of Graphene Films for Stretchable Transparent Electrodes. *Nature* **2009**, *457*, 706−710.

(17) Novoselov, K. S.; Geim, A. K.; Morozov, S. V.; Jiang, D.; Zhang, Y.; Dubonos, S. V.; Grigorieva, I. V.; Firsov, A. A. Electric Field Effect in Atomically Thin Carbon Films. *Science* **2004**, *306*, 666−669.

(18) Mao, S.; Pu, H.; Chen, J. Graphene Oxide and Its Reduction: Modeling and Experimental Progress. *RSC Adv.* **2012**, *2*, 2643−2662.

(19) Moon, I. K.; Lee, J.; Ruoff, R. S.; Lee, H. Reduced Graphene Oxide by Chemical Graphitization. *Nat. Commun.* **2010**, *1*, 73.

(20) Park, S.; Ruoff, R. S. Chemical Methods for the Production of Graphenes. *Nat. Nanotechnol.* **2009**, *4*, 217−224.

(21) Tung, V. C.; Allen, M. J.; Yang, Y.; Kaner, R. B. High-Throughput Solution Processing of Large-Scale Graphene. *Nat. Nanotechnol.* **2009**, *4*, 25−29.

(22) Yang, X.; Zhu, J.; Qiu, L.; Li, D. Bioinspired Effective Prevention of Restacking in Multilayered Graphene Films: Towards the Next Generation of High-Performance Supercapacitors. *Adv. Mater.* **2011**, *23*, 2833−2838.

(23) Luo, J.; Jang, H. D.; Sun, T.; Xiao, L.; He, Z.; Katsoulidis, A. P.; Kanatzidis, M. G.; Gibson, J. M.; Huang, J. Compression and Aggregation-Resistant Particles of Crumpled Soft Sheets. *ACS Nano* **2011**, *5*, 8943−8949.

(24) Luo, J.; Zhao, X.; Wu, J.; Jang, H. D.; Kung, H. H.; Huang, J. Crumpled Graphene-Encapsulated Si Nanoparticles for Lithium Ion Battery Anodes. *J. Phys. Chem. Lett.* **2012**, *3*, 1824−1829.

(25) Ma, X.; Zachariah, M. R.; Zangmeister, C. D. Crumpled Nanopaper from Graphene Oxide. *Nano Lett.* **2012**, *12*, 486−489.

(26) Mao, S.; Wen, Z.; Huang, T.; Hou, Y.; Chen, J. High-Performance Bi-functional Electrocatalysts of 3D Crumpled Graphene−Cobalt Oxide Nanohybrids for Oxygen Reduction and Evolution Reactions. *Energy Environ. Sci.* **2014**, *7*, 609−616.

(27) Mao, S.; Wen, Z.; Kim, H.; Lu, G.; Hurley, P.; Chen, J. A General Approach to One-Pot Fabrication of Crumpled Graphene-Based Nanohybrids for Energy Applications. *ACS Nano* **2012**, *6*, 7505−7513.

(28) Ruoff, R. A Means to an End. *Nature* **2012**, *483*, S42−S42.

(29) Ma, X.; Zachariah, M. R.; Zangmeister, C. D. Reduction of Suspended Graphene Oxide Single Sheet Nanopaper: The Effect of Crumpling. *J. Phys. Chem. C* **2013**, *117*, 3185−3191.

(30) Wang, W.-N.; Jiang, Y.; Biswas, P. Evaporation-Induced Crumpling of Graphene Oxide Nanosheets in Aerosolized Droplets: Confinement Force Relationship. *J. Phys. Chem. Lett.* **2012**, *3*, 3228−3233.

(31) Holm, R. *Electric Contacts: Theory and Application*; Springer: Berlin, 2000.

(32) Luo, J.; Jang, H. D.; Huang, J. Effect of Sheet Morphology on the Scalability of Graphene-Based Ultracapacitors. *ACS Nano* **2013**, *7*, 1464−1471.

(33) Beidaghi, M.; Wang, C. Micro-supercapacitors Based on Interdigital Electrodes of Reduced Graphene Oxide and Carbon Nanotube Composites with Ultrahigh Power Handling Performance. *Adv. Funct. Mater.* **2012**, *22*, 4501−4510.

(34) Cheng, H.; Dong, Z.; Hu, C.; Zhao, Y.; Hu, Y.; Qu, L.; Chena, N.; Dai, L. Textile Electrodes Woven by Carbon Nanotube−Graphene Hybrid Fibers for Flexible Electrochemical Capacitors. *Nanoscale* **2013**, *5*, 3428−3434.
(35) Fan, Z.; Yan, J.; Zhi, L.; Zhang, Q.; Wei, T.; Feng, J.; Zhang, M.; Qian, W.; Wei, F. A Three-Dimensional Carbon Nanotube/Graphene Sandwich and Its Application as Electrode in Supercapacitors. *Adv. Mater.* **2010**, *22*, 3723−3728.
(36) Lin, L.-Y.; Yeh, M.-H.; Tsai, J.-T.; Huang, Y.-H.; Sun, C.-L.; Ho, K.-C. A Novel Core−Shell Multi-walled Carbon Nanotube@graphene Oxide Nanoribbon Heterostructure as a Potential Supercapacitor Material. *J. Mater. Chem. A* **2013**, *1*, 11237−11245.
(37) Yan, Z.; Ma, L.; Zhu, Y.; Lahiri, I.; Hahm, M. G.; Liu, Z.; Yang, S.; Xiang, C.; Lu, W.; Peng, Z.; Sun, Z.; Kittrell, C.; Lou, J.; Choi, W.; Ajayan, P. M.; Tour, J. M. Three-Dimensional Metal−Graphene Nanotube Multifunctional Hybrid Materials. *ACS Nano* **2012**, *7*, 58−64.
(38) Yu, D.; Dai, L. Self-Assembled Graphene/Carbon Nanotube Hybrid Films for Supercapacitors. *J. Phys. Chem. Lett.* **2010**, *1*, 467−470.
(39) Zhu, Y.; Li, L.; Zhang, C.; Casillas, G.; Sun, Z.; Yan, Z.; Ruan, G.; Peng, Z.; Raji, A.-R. O.; Kittrell, C.; Hauge, R. H.; Tour, J. M. A Seamless Three-Dimensional Carbon Nanotube Graphene Hybrid Material. *Nat. Commun.* **2012**, *3*, 1225.
(40) Park, S.; An, J.; Potts, J. R.; Velamakanni, A.; Murali, S.; Ruoff, R. S. Hydrazine-Reduction of Graphite- and Graphene-Oxide. *Carbon* **2011**, *49*, 3019−3023.
(41) Bo, Z.; Zhu, W.; Ma, W.; Wen, Z.; Shuai, X.; Chen, J.; Yan, J.; Wang, Z.; Cen, K.; Feng, X. Vertically Oriented Graphene Bridging Active-Layer/Current-Collector Interface for Ultrahigh Rate Supercapacitors. *Adv. Mater.* **2013**, *25*, 5799−5806.
(42) Hughes, M.; Shaffer, M. S. P.; Renouf, A. C.; Singh, C.; Chen, G. Z.; Fray, J.; Windle, A. H. Electrochemical Capacitance of Nanocomposite Films Formed by Coating Aligned Arrays of Carbon Nanotubes with Polypyrrole. *Adv. Mater.* **2002**, *14*, 382−385.
(43) Mhamane, D.; Suryawanshi, A.; Unni, S. M.; Rode, C.; Kurungot, S.; Ogale, S. Hierarchically Nanoperforated Graphene as a High Performance Electrode Material for Ultracapacitors. *Small* **2013**, *9*, 2801−2809.
(44) Conway, B. E. *Electrochemical Supercapacitors: Scientific Fundamentals and Technological Applications*; Kluwer Academic/Plenum Publisher: New York, 1999.
(45) Burke, A. R&D Considerations for the Performance and Application of Electrochemical Capacitors. *Electrochim. Acta* **2007**, *53*, 1083−1091.
(46) Cheng, Y.; Lu, S.; Zhang, H.; Varanasi, C. V.; Liu, J. Synergistic Effects from Graphene and Carbon Nanotubes Enable Flexible and Robust Electrodes for High-Performance Supercapacitors. *Nano Lett.* **2012**, *12*, 4206−4211.
(47) Stoller, M. D.; Ruoff, R. S. Best Practice Methods for Determining an Electrode Material's Performance for Ultracapacitors. *Energy Environ. Sci.* **2010**, *3*, 1294−1301.
(48) Chen, J.; Sheng, K.; Luo, P.; Li, C.; Shi, G. Graphene Hydrogels Deposited in Nickel Foams for High-Rate Electrochemical Capacitors. *Adv. Mater.* **2012**, *24*, 4569−4573.
(49) Gao, W.; Singh, N.; Song, L.; Liu, Z.; Reddy, A. L. M.; Ci, L.; Vajtai, R.; Zhang, Q.; Wei, B.; Ajayan, P. M. Direct Laser Writing of Micro-supercapacitors on Hydrated Graphite Oxide Films. *Nat. Nanotechnol.* **2011**, *6*, 496−500.
(50) Hu, L.; Chen, W.; Xie, X.; Liu, N.; Yang, Y.; Wu, H.; Yao, Y.; Pasta, M.; Alshareef, H. N.; Cui, Y. Symmetrical MnO_2−Carbon Nanotube−Textile Nanostructures for Wearable Pseudocapacitors with High Mass Loading. *ACS Nano* **2011**, *5*, 8904−8913.
(51) Wen, Z.; Wang, X.; Mao, S.; Bo, Z.; Kim, H.; Cui, S.; Lu, G.; Feng, X.; Chen, J. Crumpled Nitrogen-Doped Graphene Nanosheets with Ultrahigh Pore Volume for High-Performance Supercapacitor. *Adv. Mater.* **2012**, *24*, 5610−5616.
(52) Gopalakrishnan, K.; Govindaraj, A.; Rao, C. N. R. Extraordinary Supercapacitor Performance of Heavily Nitrogenated Graphene Oxide Obtained by Microwave Synthesis. *J. Mater. Chem. A* **2013**, *1*, 7563−7565.
(53) Han, J.; Zhang, L. L.; Lee, S.; Oh, J.; Lee, K.-S.; Potts, J. R.; Ji, J.; Zhao, X.; Ruoff, R. S.; Park, S. Generation of B-Doped Graphene Nanoplatelets Using a Solution Process and Their Supercapacitor Applications. *ACS Nano* **2013**, *7*, 19−26.
(54) Stoller, M. D.; Park, S.; Zhu, Y.; An, J.; Ruoff, R. S. Graphene-Based Ultracapacitors. *Nano Lett.* **2008**, *8*, 3498−3502.
(55) Jeong, H. M.; Lee, J. W.; Shin, W. H.; Choi, Y. J.; Shin, H. J.; Kang, J. K.; Choi, J. W. Nitrogen-Doped Graphene for High-Performance Ultracapacitors and the Importance of Nitrogen-Doped Sites at Basal Planes. *Nano Lett.* **2011**, *11*, 2472−2477.
(56) Zhang, S.; Pan, N. Supercapacitor Performance of Crumpled and Planar Graphene Materials Produced by Hydrogen Gas Reduction of Graphene Oxide. *J. Mater. Chem. A* **2013**, *1*, 7957−7962.
(57) Wu, Z.-S.; Winter, A.; Chen, L.; Sun, Y.; Turchanin, A.; Feng, X.; Muellen, K. Three-Dimensional Nitrogen and Boron Co-doped Graphene for High-Performance All-Solid-State Supercapacitors. *Adv. Mater.* **2012**, *24*, 5130−5135.
(58) Yoo, J. J.; Balakrishnan, K.; Huang, J.; Meunier, V.; Sumpter, B. G.; Srivastava, A.; Conway, M.; Reddy, A. L. M.; Yu, J.; Vajtai, R.; Ajayan, P. M. Ultrathin Planar Graphene Supercapacitors. *Nano Lett.* **2011**, *11*, 1423−1427.